

Chemical Composition Tuning of the Anomalous Hall Effect in Isoelectronic L1₀ FePd_{1-x}Pt_x Alloy Films

P. He,^{1,2} L. Ma,¹ Z. Shi,¹ G. Y. Guo,^{3,4,*} J.-G. Zheng,⁵ Y. Xin,⁶ and S. M. Zhou^{1,2,†}

¹Department of Physics, Tongji University, Shanghai 200092, P. R. China

²Department of Physics, Fudan University, Shanghai 200433, P. R. China

³Graduate Institute of Applied Physics, National Chengchi University, Taipei 11605, Taiwan

⁴Department of Physics, National Taiwan University, Taipei 10617, Taiwan

⁵Laboratory for Electron and X-ray Instrumentation,
University of California, Irvine, CA 92697-2800, USA

⁶NHMFL, Florida State University, Tallahassee, FL 32310, USA

(Dated: May 19, 2012)

The anomalous Hall effect (AHE) in L1₀ FePd_{1-x}Pt_x alloy films is studied both experimentally and theoretically. We find that the intrinsic contribution (σ_{AH}^{int}) to the AHE can be significantly increased whereas the extrinsic side-jump contribution (σ_{AH}^{sj}) can be continuously reduced from being slightly larger than σ_{AH}^{int} in L1₀ FePd to being much smaller than σ_{AH}^{int} in L1₀ FePt, by increasing the Pt composition x . We show that this chemical composition tuning of the intrinsic contribution is afforded by the stronger spin-orbit coupling strength on the Pd/Pt site when the lighter Pd atoms are replaced by the heavier Pt atoms. Our results provide a means of manipulating the competing AHE mechanisms in ferromagnetic alloys for fuller understanding the AHE and also for technological applications of ferromagnetic alloys.

PACS numbers: 71.70.Ej; 73.50.Jt; 75.47.Np; 75.50.Bb

Anomalous Hall effect (AHE) refers to the transverse charge current generation in solids in a ferromagnetic phase generated by the electric field. The AHE, though first discovered by Hall in 1881¹, has received intensive renewed interest in recent years mainly because of its close connection with spin transport phenomena². There are several competing mechanisms proposed for the AHE. Extrinsic mechanisms of skew scattering³ and side jump⁴ result from the asymmetric impurity scattering caused by the spin-orbit interaction (SOI). Another mechanism arises from the transverse velocity of the Bloch electrons induced by the SOI, discovered by Karplus and Luttinger⁵. This intrinsic AHE has recently been reinterpreted in terms of the Berry curvature of the occupied Bloch states.⁶ Experimentally, the measured anomalous Hall resistivity ρ_{AH} is often analyzed in terms of two distinctly different resistivity (ρ_{xx})-dependent terms², i.e.,

$$\rho_{AH} = a\rho_{xx} + b\rho_{xx}^2. \quad (1)$$

Since usually $\rho_{AH} \ll \rho_{xx}$, the anomalous Hall conductivity (AHC) $\sigma_{AH} = \rho_{AH}/(\rho_{AH}^2 + \rho_{xx}^2) \approx a\sigma_{xx} + b$, where the linear σ_{xx} -dependent term ($a\sigma_{xx}$) was attributed to the extrinsic skew scattering mechanism (σ_{AH}^{sk})³. The skew scattering contribution has been found to become dominant in dilute impurity metals at low temperatures.² The scattering-independent term b was further separated into the intrinsic contribution (σ_{AH}^{int})⁵ which can be obtained from band structure calculations², and the extrinsic side jump mechanism (σ_{AH}^{sj})⁴, i.e., $b = \sigma_{AH}^{int} + \sigma_{AH}^{sj}$.

Several fundamental issues concerning the AHE remain unresolved, despite intensive theoretical and experimental studies in recent years. First-principles studies based on the Berry phase formalism showed that the intrinsic AHC agrees well with the measured scattering-

independent contribution b in various materials.^{7,8} This indicates that the side jump contribution is small, and hence the intrinsic mechanism can be assumed to be dominant². This is supported by the recent experimental finding of the negligible σ_{AH}^{sj} in fcc Ni⁹ using a newly proposed empirical σ_{xx} -scaling formula for σ_{AH} ¹⁰. However, recent theoretical calculations for the 2D Rashba and 3D Luttinger Hamiltonians using a Gaussian disorder model potential suggested that the AHE in the (III,Mn)V ferromagnetic semiconductors at low temperatures could be dominated by the σ_{AH}^{sj} .¹¹ Perhaps, most surprising is the recent report of the side jump dominant mechanism in L1₀ FePd but the intrinsic dominant mechanism in L1₀ FePt.¹² This finding was based on the σ_{AH}^{sj} deduced as the difference between the measured b and calculated σ_{AH}^{int} , and thus hinges on the accurate determination of both experimental b and theoretical σ_{AH}^{int} . However, the latest *ab initio* calculations¹³ gave the σ_{AH}^{sj} that is about three times smaller than the deduced σ_{AH}^{sj} in Ref. 12. This confusing situation on the side jump contribution to the AHC is partially caused by the fact that the σ_{AH}^{sj} is independent of the impurity concentration although it arises from the SOI-induced asymmetric electron scattering at the impurities.^{2,4,14}

All the above mentioned AHE mechanisms are caused by relativistic SOI in solids.² In particular, *ab initio* calculations showed that the intrinsic AHC depends almost linearly on the SOI strength (ξ) in, e.g., bcc Fe⁷, L1₀ FePd and L1₀ FePt¹². For better understanding of the AHE and related spin transport phenomena, it is very important to be able to experimentally tune the relative contributions of the different mechanisms to the AHC via systematic SOI engineering. To this end, isoelectronic L1₀ FePd_{1-x}Pt_x (FePdPt) ternary alloy films are ideal

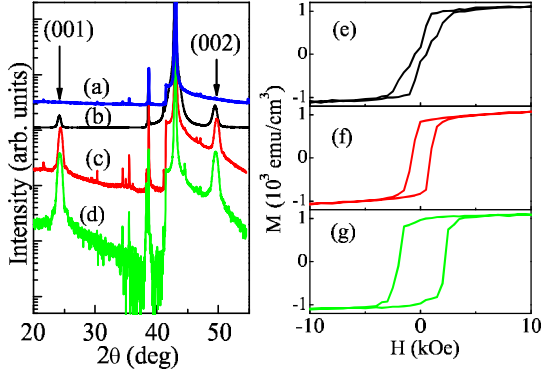


FIG. 1: (color online) XRD patterns (b, c, d) and magnetization hysteresis loops (e, f, g) for $L1_0$ $\text{FePd}_{1-x}\text{Pt}_x$ alloys with $x = 0$ (b, e), 0.65 (c, f), and 1.0 (d, g). In (a), XRD pattern of $\text{MgO}(002)$ substrate is given.

candidates because ξ could be smoothly increased several times by gradually replacing the Pd atoms with the Pt atoms while keeping other physical parameters such as crystalline structure and lattice constants almost unchanged. Therefore, extensive studies of the AHE in $L1_0$ FePdPt ternary alloys with x ranging from 0.0 to 1.0 will be crucial to establish an overall physical picture on the ξ dependence of various mechanisms and also to clarify the role of the extrinsic side jump scattering. Furthermore, these ternary alloys have promising applications to both high performance permanent magnets and ultra-high density magnetic recording media¹⁵ because of their high uniaxial magnetic anisotropy.

In this Letter, we report the different contributions to the AHC in isoelectronic $L1_0$ FePtPd alloy films. Here, we succeeded in fabricating highly ordered $L1_0$ FePdPt ternary alloy films for several different composition ratios of Pd to Pt atoms. By carefully designed experimental procedure, we determined the scattering-independent component b and skew scattering contribution for these films using the measured longitudinal and Hall resistivities as well as magnetization over a wide temperature range via the scaling formula. We performed relativistic band structure calculations to determine the intrinsic contribution. We obtained the side jump contribution by subtracting the theoretical intrinsic contribution from the experimental scattering-independent component. Our results help to better understand the competing mechanisms of the AHE in ferromagnetic alloys, a controversial issue of considerable current interest in solid state physics.

$L1_0$ $\text{FePd}_{1-x}\text{Pt}_x$ films with several different x values were deposited by DC magnetron sputtering. Details of sample fabrication, characterization of film thickness and microstructure, and measurements of magnetic properties and the anomalous Hall resistivity ρ_{AH} and longi-

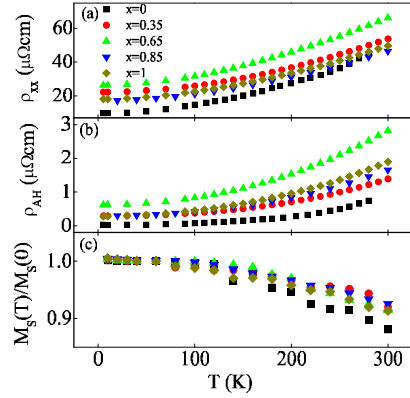


FIG. 2: (color online) ρ_{xx} (a), ρ_{AH} (b), and normalized spontaneous magnetization (c) for $L1_0$ $\text{FePd}_{1-x}\text{Pt}_x$ alloys.

tudinal resistivity ρ_{xx} are described elsewhere¹⁶. The film thickness is 20 ± 1 nm. The x-ray diffraction (XRD) peak around $2\theta = 23^\circ$ indicates the establishment of the long range chemical ordering, as shown in Figs. 1(b)-1(d). Since XRD peaks in the 2θ region from 30° to 40° come from MgO substrate, all samples are of $L1_0$ single phase. The epitaxial quality of all samples is confirmed by high resolution transmission electronic microscopy results¹⁶. For $L1_0$ FePd and FePt films, the ordering parameter $S = 0.81$ and 0.71 , respectively. For $0 < x < 1$, S lies between 0.7 and 0.8. As shown in Figs. 1(e)-1(g), the perpendicular magnetic anisotropy in the $L1_0$ -ordered FePdPt films could be tuned by varying x ^{17,18}.

The measured ρ_{xx} , ρ_{AH} and spontaneous magnetization M_S are displayed as a function of temperature (T) in Fig. 2. We find that the $\rho_{xx}(T)$ can be fitted by a linear function of T^2 , indicating the dominant electron scattering by spin flip^{19,20}. Also, the ρ_{AH} is about two orders of magnitude smaller than ρ_{xx} . The residual resistivity ρ_{xx0} [i.e., $\rho_{xx}(T = 0)$] changes non-monotonically with x and reaches the maximal value at $x = 0.65$. This may be attributed to the different crystalline quality for different Pd contents^{17,18}. Figure 2(c) shows that M_S decreases with increasing T . For all samples, the $M_S(T)$ can be fitted by a linear function of T^2 , being due to either the excitation of long wavelength spin waves or the interaction between spin waves or both^{8,21}.

To extract different contributions to the AHC using the scaling formula of Eq. (1), the ρ_{AH}/ρ_{xx} ratio is plotted as a function of ρ_{xx} in Fig. 3(a). Clearly, the ρ_{AH}/ρ_{xx} ratio deviates from the linear ρ_{xx} -dependence. This deviation arises from our experimental strategy that for a given sample, the variations of ρ_{xx} and ρ_{AH} are accomplished by varying temperature. However, varying temperature inevitably changes M_S in the sample. In Fe films which have a Curie temperature (T_C) above 1000 K, M_S hardly

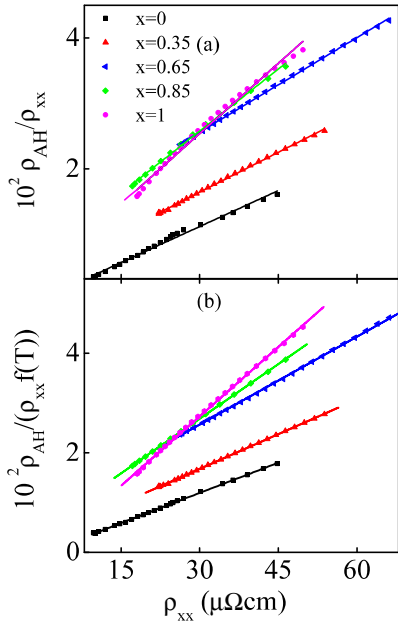


FIG. 3: (color online) ρ_{AH}/ρ_{xx} (a) and $\rho_{AH}/[\rho_{xx}f(T)]$ (b) versus ρ_{xx} for $L1_0$ $\text{FePd}_{1-x}\text{Pt}_x$ films. Solid lines in (b) refer to a linear fit.

changes with T below room temperature¹⁰. In contrast, $L1_0$ FePdPt films have a lower T_C of around 740 K²², and thus the measured M_S varies significantly with T , as shown in Fig. 2(c). Previous *ab initio* calculations and experimental studies^{8,23,24} showed that because the intrinsic AHC is proportional to M_S , the σ_{AH}^{int} and M_S have the same T -dependence [$f(T)$]. Also, the skew scattering contribution σ_{AH}^{sk} was found to be roughly proportional to M_S ¹⁴. Therefore, when using the scaling formula of Eq. (1) to fit the measured AHC, we assume $a = a_0f(T)$ and $b = b_0f(T)$ where a_0 and b_0 refer, respectively, to a and b at 0 K. The validity of the above assumption is evident in Fig. 3(b) where the $\rho_{AH}/[\rho_{xx}f(T)]$ ratio for all the samples is shown to be a perfect linear function of ρ_{xx} . The slope and the intercept of the lines are the b_0 and a_0 , respectively. This shows that, to reliably deduce b_0 and a_0 for $L1_0$ FePdPt alloy films, it is essential to take into account the T -dependence of the M_S in the T regime studied here.

To determine the intrinsic AHC, we perform self-consistent relativistic band structure calculations within the density functional theory with the generalized gradient approximation²⁵ for pure $L1_0$ FePd and FePt as well as $L1_0$ $\text{FePd}_{1-x}\text{Pt}_x$ alloys in the virtual crystal approximation¹⁶. The calculated σ_{AH0}^{int} [displayed in Fig. 4(a)] for $L1_0$ FePd and FePt is 177 and 830 S/cm, respectively, being in rather good agreement with previous *ab initio* calculations¹². Interestingly, Fig. 4(a) shows that both the experimentally derived scattering-independent term

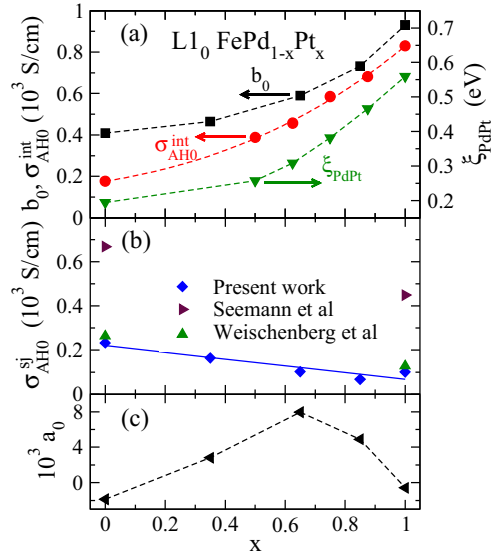


FIG. 4: (color online) Experimental b_0 , theoretical σ_{AH0}^{int} and ξ_{PdPt} (a), deduced σ_{AH0}^{sj} (b), and experimental a_0 (c) for $L1_0$ $\text{FePd}_{1-x}\text{Pt}_x$ films as a function of the Pt concentration x . In (b), the σ_{AH0}^{sj} values estimated by Seemann *et al.*¹² and calculated from first-principles by Weischenberg *et al.*¹³, are also displayed. The solid line in (b) is a linear fit.

b_0 and theoretical σ_{AH0}^{int} increase monotonically with Pt concentration x . The b_0 (σ_{AH0}^{int}) is 409 (177) and 930 (830) S/cm, respectively, for $L1_0$ FePd ($x = 0$) and $L1_0$ FePt ($x = 1$) films. This demonstrates that the AHC in the FePdPt ternary alloys, can be engineered by chemical composition tuning. To understand the mechanism of this chemical composition tuning, we display in Fig. 4(a) the calculated Pd/Pt-site d -orbital SOI strength ξ_{PdPt} as a function of x . The calculated Fe d -orbital SOI strength ξ_{Fe} of 0.061 eV is independent of x . The calculated ξ_{Pt} ($x = 1$) is 0.559 eV, being almost three times larger than the calculated ξ_{Pd} ($x = 0$) of 0.194 eV. Fig. 4(a) shows that the variations of both b_0 and σ_{AH0}^{int} with x follow closely that of $\xi_{PdPt}(x)$. Clearly, the chemical composition tuning of the AHC in $L1_0$ FePdPt films reported here is realized by substituting the Pd atoms with the heavier Pt atoms which have a stronger SOI strength.

As mentioned above, $b_0 = \sigma_{AH0}^{int} + \sigma_{AH0}^{sj}$ where σ_{AH0}^{int} and σ_{AH0}^{sj} denote σ_{AH}^{int} and σ_{AH}^{sj} at 0 K, respectively. Thus, using the measured b_0 and calculated σ_{AH0}^{int} here, we can estimate σ_{AH0}^{sj} for the $L1_0$ $\text{FePd}_{1-x}\text{Pt}_x$ alloys. To determine the σ_{AH0}^{int} for the experimental Pt concentrations, we fit a polynomial to the calculated σ_{AH0}^{int} values and find that $\sigma_{AH0}^{int} = 177 + 230x + 309x^2 + 113x^3$ S/cm gives a good fit, as the red dashed curve in Fig. 4(a) shows. The σ_{AH0}^{sj} estimated this way is displayed in Fig. 4(b). We find σ_{AH0}^{sj} for the pure $L1_0$ FePd and $L1_0$ FePt films to be 232 and 101 S/cm, respectively. These

σ_{AHO}^{sj} values are in good agreement with the corresponding theoretical values of 263 and 128 S/cm from latest *ab initio* calculations¹³. Interestingly, Fig. 4(b) shows that σ_{AHO}^{sj} decreases slightly with increasing x . Above the composition $x_c = 0.11$, σ_{AHO}^{sj} is smaller than σ_{AHO}^{int} .

Figure 4(c) shows that a_0 changes non-monotonically with x and reaches a maximal value of 0.008 at $x = 0.65$. This may be attributed to the non-monotonic variation of defect concentration (grain boundaries, line defects, microtwins, point defects and so on) with x , as is demonstrated by the variation of ρ_{xx0} in Fig. 2(a). It may also arise from the artifact that both the PtPd site disorder in the L1₀ structure and the scattering reach the maxima at intermediate x . Similar correlation between the a_0 and the impurity concentration was also observed for Fe films with different thickness¹⁰ and L1₀ FePt films treated with different annealing conditions²⁷. In the latter case, during the establishment of the chemical ordering at elevated annealing temperatures, the impurity concentration is reduced due to the improved crystalline quality, leading to the reduced residual resistivity and a_0 .

Different ξ dependences of the σ_{AHO}^{int} and σ_{AHO}^{sj} may reflect a strong difference in their distribution on the Fermi surface¹³. The σ_{AHO}^{int} is simply given as the Brillouin zone integral of the Berry curvature over the pristine crystal's occupied electronic states⁷ and is mainly contributed by certain "hot loops" in the vicinity of the intersections between different sheets of bands¹³. When the spin-orbit splitting occurs near the Fermi surface, very sharp peaks of the Berry curvature and the large σ_{AHO}^{int} are induced. For L1₀-ordered alloy films with the magnetization along the c -axis, the two degenerate t_{2g} orbitals d_{yz} and d_{zx} are lifted when ξ on the Pd/Pt atomic site is enhanced with

increasing x , leading to a significant increase of σ_{AHO}^{int} ²⁸. In contrast, since the σ_{AHO}^{sj} does not contain singularities near those band crossings but is mainly contributed by certain isolated "hot spots", it does not show a remarked sensitivity on ξ . Finally, the variation trends of the σ_{AHO}^{sj} and σ_{AHO}^{int} with x are again in agreement with the results based on massive Dirac Hamiltonian with randomly distributed weak δ -function-like spin-independent impurities¹⁴, where the $\sigma_{AHO}^{int}/\sigma_{AHO}^{sj}$ ratio is expected to change as a linear function of ξ^2 .

In summary, we have determined the competing contributions to the AHC in isoelectronic L1₀ FePd_{1-x}Pt_x alloy films. We found that the scattering independent component (intrinsic contribution) to the AHC can be continuously tuned from 409 (177) S/cm for L1₀ FePd ($x = 0$) to 930 (830) S/cm for L1₀ FePt ($x = 1$) by increasing the Pt composition x whereas the extrinsic side-jump contribution decreases slightly from being slightly larger than σ_{AH}^{int} at $x = 0$ to being much smaller than σ_{AH}^{int} at $x = 1$. We have related this chemical composition tuning of the intrinsic contribution to the modification of the SOI strength on the Pd/Pt site when the lighter Pd atoms are replaced by the heavier Pt atoms. Our results would help better understand the origins of various mechanisms of the AHE in ferromagnetic alloys and also pay the way for designing the broad class of ferromagnetic L1₀ XPdPt (X=Fe and Co) ternary alloys^{29,30} for spintronic devices and magnetic sensors.

This work was supported by the National Natural Science Foundation of China, the National Basic Research Program of China, the National Science Council of Taiwan, FSU Research Foundation and NHMFL (NSF DMR-0654118).

* Electronic address: gyguo@phys.ntu.edu.tw

† Electronic address: shiming@tongji.edu.cn

¹ E. H. Hall, *Philos. Mag.* **12**, 157 (1881)

² N. Nagaosa *et al.*, *Rev. Mod. Phys.* **82**, 1539 (2010)

³ J. Smit, *Physica (Amsterdam)* **21**, 877 (1958); **24**, 39 (1958)

⁴ L. Berger, *Phys. Rev. B* **2**, 4559 (1970)

⁵ R. Karplus and J. M. Luttinger, *Phys. Rev.* **95**, 1154 (1954)

⁶ D. Xiao, M.-C. Chang, and Q. Niu, *Rev. Mod. Phys.* **82**, 1959 (2010)

⁷ Y. G. Yao *et al.*, *Phys. Rev. Lett.* **92**, 037204 (2004)

⁸ C. G. Zeng *et al.*, *Phys. Rev. Lett.* **96**, 037204 (2006)

⁹ L. Ye *et al.*, arXiv:1105.5664.

¹⁰ Y. Tian, L. Ye, and X. F. Jin, *Phys. Rev. Lett.* **103**, 087206 (2009)

¹¹ A. A. Kovalev, J. Sinova, and Y. Tserkovnyak, *Phys. Rev. Lett.* **105**, 036601 (2010)

¹² K. M. Seemann *et al.*, *Phys. Rev. Lett.* **104**, 076402 (2010)

¹³ J. Weischenberg *et al.*, *Phys. Rev. Lett.* **107**, 106601 (2011)

¹⁴ N. A. Sinitsyn *et al.*, *Phys. Rev. B* **75**, 045315 (2007)

¹⁵ S. Sun *et al.*, *Science* **287**, 1989 (2000)

¹⁶ See supplemental material at

<http://link.aps.org/supplementary/> for further experimental and computational details.

¹⁷ S. Jeong *et al.*, *J. Appl. Phys.* **91**, 8813 (2002)

¹⁸ G. J. Chen *et al.*, *Surf. Coat. Technol.* **202**, 937 (2007)

¹⁹ M. J. Otto *et al.*, *J. Phys.: Condens. Matter* **1**, 2351 (1989)

²⁰ I. Mannari, *Prog. Theor. Phys.* **22**, 335 (1959)

²¹ G. G. Lonzarich and L. Taillefer, *J. Phys. C* **18**, 4339 (1985)

²² S. Okamoto *et al.*, *Phys. Rev. B* **66**, 024413 (2002)

²³ B. C. Sales *et al.*, *Phys. Rev. B* **73**, 224435 (2006)

²⁴ A. Husmann and L. J. Singh, *Phys. Rev. B* **73**, 172417 (2006)

²⁵ J. P. Perdew, K. Burke, and M. Ernzerhof, *Phys. Rev. Lett.* **77**, 3865 (1996)

²⁶ W. J. Jiang, X. Z. Zhou, and G. Williams, *Phys. Rev. B* **82**, 144424 (2010)

²⁷ M. Chen *et al.*, *Appl. Phys. Lett.* **98**, 082503 (2011)

²⁸ H. B. Zhang, S. Blügel, and Y. Mokrousov, *Phys. Rev. B* **84**, 024401 (2011)

²⁹ S. S. Kang, *et al.*, *J. Appl. Phys.* **95**, 6744 (2004)

³⁰ S. Susumu, U. S. Patent, No. 20080074776 (2008)